Neuromuscular fatigue and recovery after strenuous exercise depends on skeletal muscle size and stem cell characteristics

Baumert, P.[1,2]*, Temple, S.[1], Stanley, J.M.[1], Cocks M. [1], Strauss, J.A. [1], Shepherd S.O.[1], Drust, B.[1], Lake, M.J.[1], Stewart, C.E.[1], Erskine, R.M.[1,3]

[1]*Research Institute for Sport & Exercise Sciences, Liverpool John Moores University, Liverpool, United Kingdom.*

[2]*Exercise Biology Group, Faculty of Sport and Health Sciences, Technical University of Munich, Munich, Germany*

[3]*Institute of Sport, Exercise & Health, University College London, London, UK*

Running title: Neuromuscular Response following muscle damage *in vivo* and *in vitro*

Address for reprint requests and all other correspondence:

Philipp Baumert, Exercise Biology Group, Faculty of Sport and Health Sciences, Technical University of Munich, Munich, Germany; Email: philipp.baumert@tum.de

Key words: Exercise-induced muscle damage (EIMD); biceps femoris architecture; extracellular matrix (ECM); myoblast; fibroblast

This is an original research article

ABSTRACT

Hamstring muscle injury is highly prevalent in sports involving repeated maximal sprinting. Although neuromuscular fatigue is thought to be a risk factor, the mechanisms underlying the fatigue response to repeated maximal sprints are unclear. Here, we show that repeated maximal sprints induce neuromuscular fatigue accompanied with a prolonged strength loss in hamstring muscles. The immediate hamstring strength loss was linked to both central and peripheral fatigue, while prolonged strength loss was associated with indicators of muscle damage. The kinematic changes immediately after sprinting likely protected fatigued hamstrings from excess elongation stress, while larger hamstring muscle physiological cross-sectional area and lower *myoblast:fibroblast* ratio appeared to protect against fatigue/damage and improve muscle recovery within 48 h after sprinting. Contrastingly, a high *myoblast:fibroblast* ratio appears crucial for the latter stage of muscle regeneration. We have therefore identified novel mechanisms that likely regulate the fatigue/damage response and recovery following repeated maximal sprinting in humans.

INTRODUCTION

Hamstring strain is the most frequently occurring injury in sport (Crema *et al.*, 2017), particularly in those sports that involve high-speed running (Ekstrand *et al.*, 2011; Opar *et al.*, 2012). Although the aetiology is unclear, numerous risk factors have been proposed, such as short fascicle length (Timmins *et al.*, 2015), poor flexibility (Jonhagen *et al.*, 1994), poor hamstring strength (Opar *et al.*, 2014), and inadequate warm-up (Woods *et al.*, 2007). Further, it is unknown whether hamstring strain is a result of a single event that exceeds the physiological range of hamstring muscle extensibility and contractility, or as a result of an accumulation of eccentric contractions during repeated maximal sprints, causing neuromuscular fatigue (Opar *et al.*, 2012). Neuromuscular fatigue is responsible for acute, as well as prolonged, impairment of muscle function and it can be classified as central fatigue (i.e. originating in the central nervous system), or as peripheral fatigue (i.e. distal to the neuromuscular junction) (Byrne *et al.*, 2004). Although it was recently reported that both central and peripheral fatigue contribute to impaired hamstring muscle function immediately after repeated maximal sprint-related interventions (Marshall *et al.*, 2014; Timmins *et al.*, 2014), the contribution of neuromuscular fatigue to hamstring muscle impairment and recovery over time is insufficiently studied following repeated maximal sprints (Verma *et al.*, 2015). An understanding of hamstring neuromuscular fatigue following repeated maximal sprints may be crucial for understanding hamstring strain aetiology (van der Horst *et al.*, 2015).

Peripheral fatigue may be caused by ultrastructural muscle damage, which is indicated by Z-line disturbance (Newham *et al.*, 1983) as well as disruption of the extracellular matrix (Stauber *et al.*, 1990). The extracellular matrix provides structural scaffolding for muscle remodelling and plays an integral role in force transmission (Wang *et al.*, 2009; Gillies & Lieber, 2011). This is referred to as exercise-induced muscle damage and it is exhibited by prolonged strength loss and delayed-onset muscle soreness, as well as the release of muscle-specific proteins [e.g. creatine kinase (CK)] into the circulation over the following days (Howatson & Van Someren, 2008). After substantial muscle damage, myogenic satellite cells (skeletal muscle

stem cells), play a key role in skeletal muscle regeneration and remodelling, as activated satellite cells (myoblasts) proliferate and migrate from their niche along the basal lamina to the injury site before terminally differentiating and fusing into myotubes (Tidball, 2011). There is increasing evidence that fibroblasts, the main cell type of muscle connective tissue, play a critical role in supporting muscle regeneration (Murphy *et al.*, 2011; Fry *et al.*, 2017; Mackey *et al.*, 2017). Following damage, infiltrating inflammatory cells activate muscle fibroblasts, which proliferate and migrate to the area of the myotrauma and produce extracellular matrix components in an orchestrated and regulated fashion to support healthy muscle remodelling (Joe *et al.*, 2010; Murphy *et al.*, 2011). However, less is known about the effect of fibroblasts on the initial response and recovery following *physiological* exercise-induced muscle damage, e.g. following repeated sprinting.

This acute damage to the muscle-tendon complex may facilitate hamstring strain, which is thought to occurs in the late swing phase of sprinting, when the hamstring muscles contract eccentrically, i.e. trying to shorten while being lengthened in an attempt to decelerate the shaft before initial foot-ground contact (Thelen *et al.*, 2005; Chumanov *et al.*, 2012). Therefore, a short biceps femoris long head (BF_{LH}) fascicle length has been suggested to increase hamstring strain risk (Timmins *et al.*, 2016a), as the BF_{LH} is thought to be relatively more eccentrically stretched during the late swing phase of sprinting compared to the other hamstring muscles (Thelen *et al.*, 2005). However, no study has investigated the relationship between BF_{LH} architecture (including muscle fascicle length and cross-sectional area), and the prolonged hamstring muscle response to exercise-induced neuromuscular fatigue. Finally, lower limb neuromuscular fatigue might cause a number of biomechanical alterations in running kinematics (Paschalis *et al.*, 2007). However, it is not known whether repeated maximal sprints influence kinematic patterns, and whether this can lead to prolonged changes in lower-limb kinematics, which may play a role in the development of muscle strain following insufficient recovery (Opar *et al.*, 2012).

Here we demonstrated that both central and peripheral fatigue contributed to the immediate loss of muscle function in both the quadriceps and hamstring muscle groups, but that peripheral factors mainly contributed to the sustained loss of hamstring muscle function. Moreover, we established that a lower myoblast:fibroblast ratio in isolated primary human muscle stem cells correlated with improved recovery from both repeated maximal sprints and an *in vitro* artificial wounding assay within the first 48 h. However, at seven days post damage, a higher myoblast:fibroblast ratio appears important for optimal muscle regeneration. We also found that BF_{LH} architecture (i.e. PCSA) was associated with hamstring fatigue, and that neuromuscular fatigue led to reduced hip flexion and knee extension during the late swing phase of steady-state running. Thus, with this interdisciplinary study, we identify novel cellular and neuromuscular mechanisms underpinning central and peripheral fatigue following repeated sprinting, which ultimately led to kinematic changes during the running stride phase associated with hamstring strain injury.

RESULTS

Effect of the Repeated Maximal Sprint Intervention on Neuromuscular Fatigue

To begin examining the effect of repeated maximal sprints on neuromuscular fatigue, we measured different fatigue parameters before (PRE), immediately after (POST), and 48 h after (POST48) the repeated maximal sprint intervention. The average 30 m sprinting speed was 6.48 ± 0.33 m s^{-1}. There was a main effect of time for heart rate, 30 m sprinting time, rating of perceived exertion and lactate, with all parameters increasing from PRE to POST repeated maximal sprints (all $P < 0.001$). Blood lactate concentration also increased from PRE (1.63 ± 0.45 mmol/L) to POST (9.82 ± 3.62 mmol/L). The sprinting performance (measured via the performance decrement score (Glaister *et al.*, 2008)) decreased by 3.98 ± 2.99 %, and rating of perceived exertion increased by 96.5 ± 35.2 % from PRE-to-POST, indicating fatigue had occurred.

We then performed *in vivo* functional analysis to assess if repeated maximal sprints resulted in an increase in central and/or peripheral fatigue. We, therefore, measured BF_{LH} muscle activation via normalised surface electromyography (sEMG) during hamstring maximum voluntary contraction (MVC). That assessment showed that a change had occurred in sEMG ($F_{F2,24}$=4.35, P=0.022), with post-hoc pairwise comparisons revealing a decrease from PRE-to-POST (P=0.019). However, this change was no longer evident at POST48 (P=0.157, Table 1), suggesting that central fatigue occurred immediately after repeated maximal sprints. No other changes in muscle (co)activation were observed at any time point (P>0.05).

Table 1 *Effect of the intermitted sprint intervention on measures of muscle activation. Data are presented as mean ± SD. One-way ANOVA, F- and P-values are reported.*

Assessment [unit]	n	PRE	POST	POST48	F-Test	P Value
Hamstring Muscle Voluntary Activation [ITT, %]	20	98.5 ± 2.64	94.1 ± 7.83	96.9 ± 5.96	F(1.4,38) = 2.75	0.099
Normalised BF_{LH} knee flexion $sEMG_{max}$ [%]	14	3.32 ± 1.33	2.27 ± 0.72*****	2.85 ± 1.16	F(2,24) = 4.35	0.022
Vastus lateralis knee extension $sEMG_{max}$ [mV]	15	0.50 ± 0.29	0.47 ± 0.34	0.51 ± 0.34	F(2,24) = 0.17	0.772
Quadriceps CoA during 30° hamstring MVC [%]	12	5.74 ± 7.23	4.08 ± 6.86	4.33 ± 8.76	F(2,22) = 0.50	0.613
Hamstring CoA during 80° quadriceps MVC [%]	10	4.79 ± 3.37	6.62 ± 3.79	7.51 ± 4.16	F(2,18) = 1.64	0.223

ITT – interpolated twitch technique; BF_{LH} – Biceps femoris long head; CoA – Co-Activation; sEMG – surface Electromyography. * Different to PRE (P<0.05).

We also assessed the torque-frequency relationship *in vivo* via electrical stimulation, as it gives an indication of peripheral (muscle) fatigue. There was an interaction between time x stimulation frequency (n=19; $F_{4.9,216}$=6.62, P<0.001; Figure 1A). Post-hoc paired t-tests revealed differences PRE-to-POST for 10-50 Hz, but lower frequencies between 10-20 Hz

reverted to baseline values POST48 (P>0.05), while the frequencies of 30 and 50 Hz were still decreased POST48 compared to their baseline values (P<0.05), providing evidence that peripheral fatigue occurred immediately after the repeated sprints and remained for 48 h

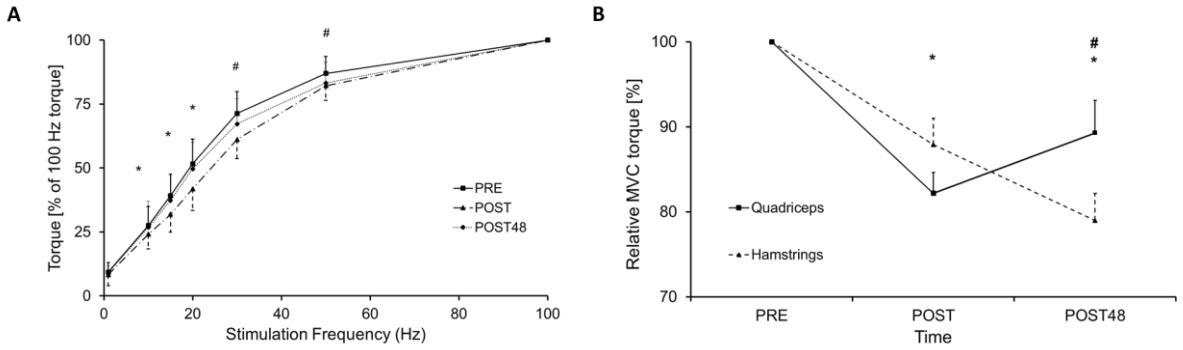

Figure 1 (A) *Torque-frequency relationship, all frequencies were normalised to 100 Hz. * significant differences between before (PRE) and immediadtely after (POST) the repeated maximal sprint intervention, P<0.05; # significant differences between PRE and POST, and between PRE and POST48, P<0.05. Data are presented as mean ± SEM.* ***(B)*** *Comparison of relative maximal voluntary contraction (MVC) loss between hamstring and quadriceps muscle group before (PRE), immediately after (POST) and 48h after (POST48) the repeated maximal sprint intervention. * signifcant differences compared to PRE, P< 0.001; # significant differences between quadriceps and hamstring MVC, P< 0.05. Data are expressed as mean ± SEM.*

Effect of the Repeated Maximal Sprint Intervention on MVC Strength, Muscle Soreness and Serum Markers of Exercise-Induced Muscle Damage

To investigate the effect of intermittent sprints on biomarkers of exercise-induced muscle damage, we assessed hamstring (knee flexion) and quadriceps (knee extension) MVC, muscle soreness, serum creatine kinase (CK) activity and interleukin-6 (IL-6) concentration PRE, POST and POST48. Isometric hamstring and quadriceps MVC, muscle soreness (all P<0.001) and serum CK activity ($F_{1.3,34}$=5.98, P=0.017), as well as IL-6 concentration ($F_{1.3,34}$=5.96, P=0.018), showed a main effect of time, which are indicators of muscle damage (Table 2) that was similar to other studies (Howatson & Milak, 2009; Verma *et al.*, 2015; Chen *et al.*, 2017). Post-hoc pairwise comparisons revealed that, compared to PRE, both serum CK activity and serum IL-6 concentration were elevated at POST (both P=0.027), and CK activity further

150 increased at POST48 (P=0.012), while serum IL-6 concentration reverted to baseline values
151 (P>0.05).

152 ***Table 2*** *Effect of the Repeated Maximal Sprint Intervention on Muscle Damage-Biomarkers. Values*
153 *are mean ± SD. One-way ANOVA, F- and P-values are reported.*

Assessment [unit]	**PRE**	**POST**	**POST48**	**F-Test**	**P Value**
Quadriceps MVC [N·m]	270.5 ± 51.6*	222.4 ± 52.5*	243.0 ± 71.3*	F(2,38) = 16.55	<0.001
Hamstring MVC [N·m]	142.5 ± 25.0*	124.8 ± 29.9*	112.4 ± 30.1*	F(2,38) = 25.12	<0.001
Squat Muscle soreness [cm]	0.20 ± 0.41*	1.95 ± 1.61*	2.87 ± 1.71*	F(2,38) = 28.62	<0.001
Lunge Muscle soreness [cm]	0.30 ± 0.57	2.30 ± 2.08†	3.48 ± 2.07†	F(2,38) = 17.02	<0.001
Range of Motion [°]	120.3 ± 6.76	115.7 ± 6.77†	116.0 ± 6.27†	F(2,38) = 9.33	<0.001
CK activity [mU/mL]	27.9 ± 23.3	53.8 ± 45.3†	99.3 ± 104.5†	F(1.3,34) = 5.98	0.017
IL-6 concentration [pg/mL]	1.89 ± 3.10	7.68 ± 9.95#	1.59 ± 3.46	F(1.3,34) = 5.96	0.018

MVC – Maximal voluntary contraction; CK – Creatine Kinase; IL-6 – Interleukin-6; * Significant differences between all time points; † differences PRE–to-POST and PRE-to-POST48 (P<0.05); # differences PRE-to-POST and POST-to-POST48 (P<0.05).

154 Further, there was an interaction between time and muscle groups concerning relative MVC
155 torque loss (percentage change from PRE MVC) ($F_{1.4,38}$=7.92, P=0.004). Relative MVC
156 decreased similarly in both quadriceps and hamstring muscle groups PRE-to-POST (Figure
157 1B). However, at POST48, hamstring MVC continued to decrease from POST (P=0.010), while
158 quadriceps MVC began to return to PRE values (P=0.016), and was higher than hamstring
159 MVC at POST48 (P=0.038).

Effect of the Repeated Maximal Sprint Intervention on Lower-Limb Kinematics

To assess the consequential effect of neuromuscular fatigue on lower-limb kinematics, we captured treadmill running (4.17 m s^{-1}) kinematics with an eight-camera motion capture system over time. Three-dimensional motion analysis showed that there was a non-significant tendency for the duration of the running cycle to take longer POST and POST48, compared to PRE (P=0.080; Table 3). Further, treadmill running demonstrated decreases in peak knee extension (P=0.047) during the late swing phase at POST compared to PRE, but this reverted to baseline POST48. The percentage change in peak knee extension correlated with the percentage change in relative hamstring MVC torque both measured POST-to-POST48 (r^2=0.258, $F_{1,2}$=5.673, P=0.031).

Table 3 *Effect of the Repeated Maximal Sprint Intervention on Kinematics of Treadmill Running at 4.17 m s^{-1} Values are mean ± SD. One-way ANOVA, F- and P-values are reported.*

Kinematics [unit]	PRE	POST	POST48	F-Test	P Value
Peak knee flexion (swing phase) [°]	-103 ± 13.9	-110 ± 12.4	-108 ± 12.6	F(2,20) = 2.84	0.082
Peak knee extension (swing phase) [°]	-3.66 ± 5.32	-7.08 ± 5.07*	-4.29 ± 7.06	F(2,20) = 3.57	0.047
Contact hip flexion (toe strike) [°]	25.2 ± 5.42	29.3 ± 7.62	17.6 ± 15.6	F(1.2,20) = 4.05	0.062
Contact knee flexion (toe strike) [°]	-15.0 ± 6.25	-17.6 ± 6.79	-13.3 ± 9.64	F(2,22) = 2.79	0.083
Duration Running cycle [s]	0.67 ± 0.03	0.68 ± 0.03	0.69 ± 0.02	F(2,20) = 2.88	0.080
Stance phase duration [s]	0.18 ± 0.02	0.19 ± 0.02	0.19 ± 0.03	F(2,20) = 1.01	0.356
Swing Phase [s]	0.50 ± 0.04	0.50 ± 0.05	0.50 ± 0.03	F(1.2,20) = 0.03	0.899

Knee fully extended=0°; negative value indicates a flexed knee; * different to PRE (P<0.05).

Architecture of the Biceps Femoris Long Head Muscle

To assess whether architectural parameters of the BF_{LH} muscle (Figure 2A and B) were associated with markers of peripheral fatigue, we performed ultrasound measurements of the BF_{LH} muscle (Table supplement 5). Muscle fascicle length and pennation angle of the BF_{LH}, which have previously been linked to hamstring muscle strain risk (Timmins *et al.*, 2016b), did not correlate with any outcome variable of neuromuscular fatigue. However, BF_{LH} PCSA (mean ±SD: 23.4 ± 4.62 cm^2) correlated inversely with relative hamstring MVC loss PRE-to-POST (R^2=0.421, $F_{1,17}$=12.37, P=0.003, Figure 2C).

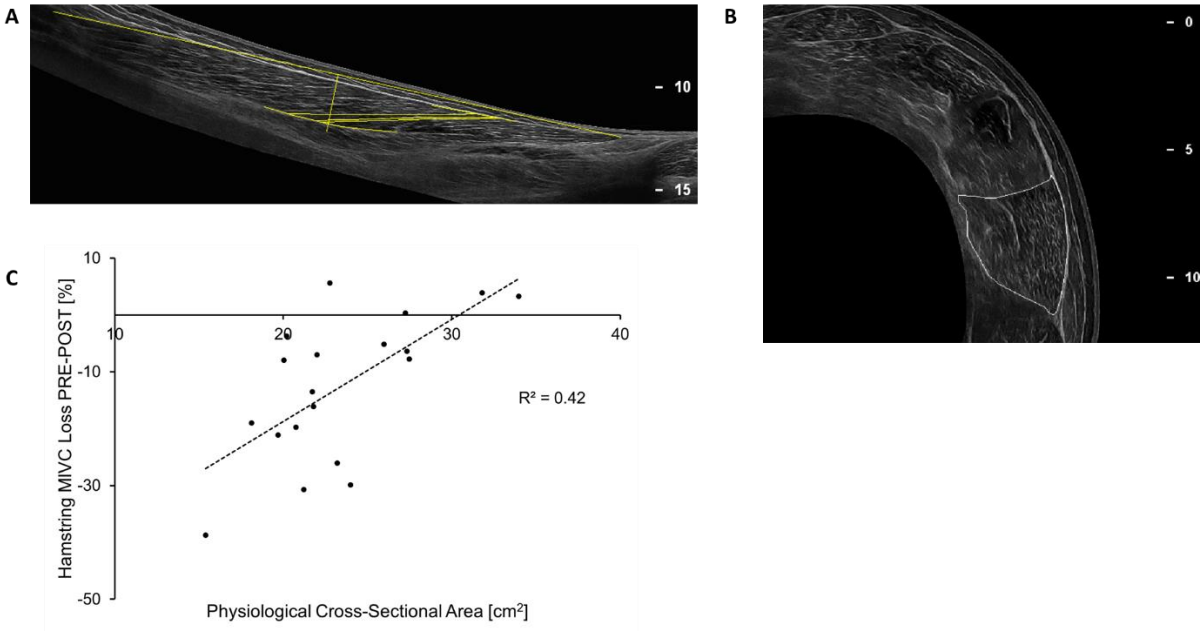

Figure 2 (A) *Longitudinal image of biceps femoris long head, assessment of the biceps femoris long head is highlighted (total muscle length and fascicle length together with pennation angle at 50% of total muscle length).* ***(B)*** *Cross-sectional image at 60% muscle length (=100% proximal myotendinous junction), biceps femoris long head is highlighted.* ***(C)*** *Correlation between biceps femoris long head muscle physiological cross-sectional area and % hamstring maximum isometric voluntary contraction (MIVC) decrease from before (PRE) to immediately after (POST) the repeated maximal sprint intervention (P=0.003).*

Comparison of the Muscle Response between the Repeated Maximal Sprint Protocol and the Muscle Stem Cell Study

We next sought to determine whether skeletal muscle stem cell composition (i.e. myoblast:fibroblast ratio) played a role in muscle strength recovery. Six of the 20 participants, who performed the repeated maximal sprint intervention, also volunteered to provide a muscle biopsy at least three weeks before the repeated maximal sprint intervention. As previous investigations have shown that skeletal muscles of different origin, but with similar physiological functions and fibre type composition, demonstrate similar transcriptome expression patterns of up to 99% (Evangelidis *et al.*, 2016; Terry *et al.*, 2018), we have taken a muscle biopsy from the vastus lateralis as a representative muscle of the quadriceps and hamstring muscle groups. The muscle stem cells were isolated, cultured and then characterized by immunofluorescence staining. The mean ± SD myoblast:fibroblast ratio of the six participants was 1.46 ± 1.06 (range: 0.299 to 2.93). There was a strong inverse correlation

between myoblast:fibroblast ratio and the percentage change in relative hamstring MVC torque measured PRE-to-POST48 *in vivo* (R=-0.945, $F_{1,4}$=33.73, P=0.004; Figure 3A). Thus, the myoblast:fibroblast ratio explained 89% of the variability in strength recovery PRE-to-POST48, i.e. participants with a high myoblast:fibroblast ratio showed a delayed hamstring strength recovery 48 h after repeated maximal sprints compared to those with a low myoblast:fibroblast ratio. Further, there was an inverse correlation between myoblast:fibroblast ratio and relative hamstring MVC torque measured POST-to-POST48 (R=-0.943, $F_{1,4}$=17.08, P=0.014; Figure 3B). Thus, the myoblast:fibroblast ratio explained 81% of the variability in strength recovery POST-to-POST48. No correlations were found between the myoblast:fibroblast ratio and changes in quadriceps MVC torque or with any other muscle damage and fatigue biomarker following repeated maximal sprints.

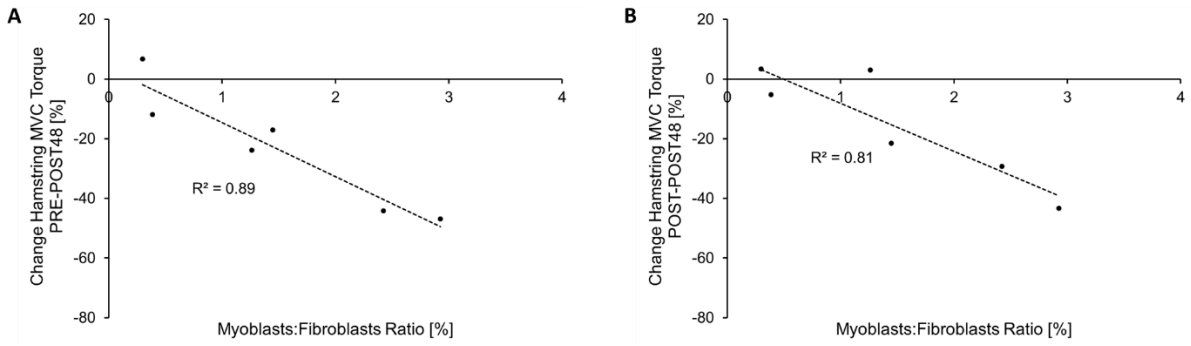

Figure 3 *Inverse correlation between the myoblast:fibroblast ratio, assessed in the current in vitro study and the change of hamstring MVC torque measured* ***(A)*** *before and 48 h after (P=0.004), and* ***(B)*** *measured immediately after and 48 h after (P=0.014) (B) the repeated maximal sprint intervention.*

Artificial Wound Healing Assay to Investigate Repair and Regeneration Regarding Myoblast:Fibroblast Ratio

To further assess the effect of the myoblast:fibroblast ratio on skeletal muscle recovery, we performed an *in vitro* artificial wounding (scratch) assay. We used primary human skeletal muscle stem cells derived from the six volunteers, who participated in both the repeated maximal sprint intervention and volunteered to provide a muscle biopsy, and another six (two male and four females), who did not participate in the repeated maximal sprint intervention (to

increase the power of the *in vitro* study). We did not detect any differences in muscle stem cell characteristics between cells obtained from females and males (data not shown). We, therefore, combined the data from all muscle cells and correlated the muscle characteristics with individual myoblast:fibroblast ratios. We observed no correlations regarding myoblast:fibroblast ratio and the total number of myoblasts and fibroblasts migrating into the artificial wound within all three segments combined at 24 h (R^2=0.20, $F_{1,10}$=2.56, P=0.141) or 48 h (R^2=0.02, $F_{1,10}$=0.19, P=0.671) after the scratch assay.

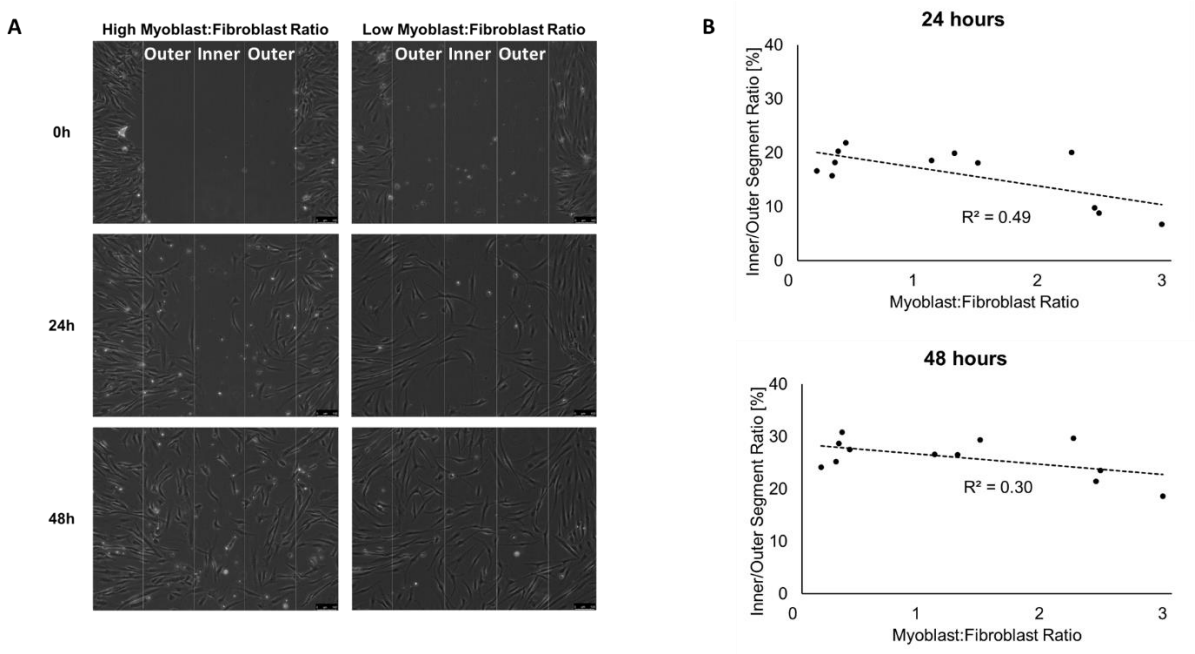

Figure 4 (A) *Representative images for cell migration of muscle cells with a high myoblast:fibroblast ratio (2.4; left) and with a low percentage of myoblasts (0.3; right) into the artificial wound. The wound area is about 900 µm in width and split into 3 x 300 µm segments (one inner and two outer segments). Magnification is x 10.5, and scale bar is 100 µm.* ***(B)*** *Inverse correlations between the myoblast:fibroblast ratio and the migration dynamics of 12 different primary muscle stem cells 24 h (P=0.011) and a trend 48 h (P=0.064) after the artificial wound healing assay.*

However, there was an inverse correlation between myoblast:fibroblast ratio and migration dynamics for the 12 participants (Figure 4 B). Muscle stem cells with a low myoblast:fibroblast ratio demonstrated more cells in the inner segment than to the outer segment compared to muscle stem cells with high myoblast:fibroblast ratio at 24 h (R^2=0.49, $F_{1,10}$=9.53, P=0.011) and with a non-significant trend at 48 h (R^2=0.30, $F_{1,10}$=4.33, P=0.064) after the artificial wound healing assay. Further, there were positive correlations between the myoblast:fibroblast ratio and all parameters at seven and 10 days after the artificial wound healing assay (all P<0.05;

Table supplement 6). Biopsies with a higher myoblast:fibroblast ratio showed more myotubes per field, which had a higher diameter and area compared to biopsies with a lower myoblast:fibroblast ratio (Figure supplement 5).

DISCUSSION

In this study, we have used an interdisciplinary approach to systematically investigate the biomechanical, physiological and cellular factors underpinning neuromuscular fatigue following repeated maximal sprints. We have shown that immediate strength loss was associated with reduced hamstring sEMG activity (indicating impaired hamstring motor unit recruitment) and markers of peripheral fatigue, but the magnitude and sustained changes in MVC torque over time (especially of the hamstrings) was largely associated with indicators of peripheral fatigue. Muscle damage biomarkers indicated that the peripheral fatigue might have been caused predominantly by ultrastructural damage within the hamstring muscle tissue. Further, both central and peripheral fatigue caused by repeated maximal sprints appeared to affect the neuromuscular control of running patterns and BF_{LH} PCSA correlated inversely with the change in hamstring MVC torque immediately after the repeated maximal sprint intervention. A high myoblast:fibroblast ratio showed a delayed wound closure *in vitro* and a delayed MVC torque recovery following repeated maximal sprints *in vivo* within the first 48 h, indicating that stem cells of the non-contractile muscle tissue might positively affect the response to muscle damaging exercises. However, a higher myoblast:fibroblast ratio led to better myotube formation at seven days, and higher CK activity at ten days, after the scratch assay, suggesting that myoblasts are important for the latter stage of muscle regeneration.

Fatigue and Muscle Damage Following Repeated Maximal Sprints

We showed a decreased activity of normalised BF_{LH} sEMG activity immediately after the repeated maximal sprint intervention, but no significant changes in neuromuscular activation using the interpolated twitch technique. The discrepancy between these two methods might

be explained by the fact that voluntary activation measured via the interpolated twitch technique investigates all of the hamstring muscles, whilst the normalised EMG analysis was confined solely to the BF_{LH}, which is in line with a previous study (Marshall *et al.*, 2014). We assume that BF_{LH} might fatigue to a greater degree immediately after repeated maximal sprint related interventions compared to the other hamstring muscles. However, we also provide evidence for peripheral fatigue occurring immediately after the repeated maximal sprints, and a delayed recovery at higher frequencies (30-50 Hz) after observing a right shift in the torque-frequency relationship. This may be due to ultrastructural damage predominantly in fast-twitch (which fire at rates from 30-50 Hz) compared to slow-twitch muscle fibres (discharge rates 10-25 Hz) (Friden *et al.*, 1983; Jones *et al.*, 1986), leading to impaired force generation rather than simply fatiguing the muscle fibres.

Both the quadriceps and hamstring muscle groups showed similar strength loss immediately after the repeated maximal sprints, but the hamstring muscle group showed further strength loss 48 h later compared to the quadriceps. Other studies did not show this additional strength loss for the hamstring muscle group POST48. Differences in the training status of the participants (Verma *et al.*, 2015; Chen *et al.*, 2017) and in the methodological approaches (Balsom *et al.*, 1992) might partly explain the different outcomes. The peak BF_{LH} EMG activity occurs at a more extended knee angle during hamstring isokinetic muscle contraction compared to the peak EMG occurring at a more flexed knee angle for the other hamstring muscles, such as the semitendinosus (Onishi *et al.*, 2002). Therefore, we suggest that the BF_{LH} is the key hamstring muscle responsible for decelerating the shaft at the end of the late swing phase. After repeated bouts of high-speed running, the semitendinosus might fatigue prematurely (Schuermans *et al.*, 2014) and the BF_{LH} would need to substitute the impaired function of the preceding semitendinosus to decelerate the shaft.

Kinematic Analysis

Our *in vivo* intervention caused changes in the running kinematics with reduced knee extension in the late swing phase immediately after the repeated maximal sprints. Reduced hamstring

298 muscle strength due to neuromuscular fatigue might trigger a protective mechanism directly
299 after repeated maximal sprints. Afferent signals from the fatigued and damaged hamstrings
300 might activate the Golgi tendon organ (Byrne *et al.*, 2004), thus limiting hamstring muscle fibre
301 strain in an attempt to minimise further muscle damage. These kinematic changes were not
302 evident 48 h after the repeated maximal sprints. However, there was a non-significant tendency
303 for prolonged stride duration during running (P = 0.08, data not shown) 48 h later and the
304 percentage change of knee extension in the late swing phase of running correlated with
305 changes in hamstring strength both measured from POST to POST48. This indicates that
306 participants with delayed hamstring strength recovery were still not able to fully control running.
307 As hamstring MVC continued to deteriorate 48 h after intermittent sprints but quadriceps MVC
308 started to improve, it could be that lower-limb kinematics in the sagittal plane are controlled by
309 the hamstrings more than the quadriceps. Ultrastructural damage in the hamstring muscles
310 might lead to decelerated movement patterns over time, which could increase the risk for
311 hamstring strain injury during sprinting (Opar *et al.*, 2012).

312 **The Role of the Extracellular Matrix on the Muscle Response Following Repeated**
313 **maximal sprinting**

314 Recent investigations have suggested that hamstring maximum eccentric strength and BF_{LH}
315 fascicle length are predictors of hamstring strain injury (Timmins *et al.*, 2016a). Further, a
316 fatigued muscle is likely to accentuate the risk of muscle strain (Ekstrand *et al.*, 2011). However,
317 we could not find any correlation between BF_{LH} fascicle length and any biomarker of fatigue
318 but BF_{LH} PCSA correlated inversely with hamstring strength loss from PRE to POST. During
319 the late swing phase of sprinting, the hamstring muscles muscles contract eccentrically to
320 decelerate the shaft and to enhance the subsequent concentring shortening contraction for
321 maximal sprinting by using stored elastic energy from the muscle-tendon unit. In comparison
322 to other conventional muscle-damaging interventions (Franchi & Maffiuletti, 2019), this
323 dynamic (stretch-shortening) movements might lead to an additional damage of the hamstring
324 muscle connective tissue structure. Therefore, a larger BF_{LH} PCSA might protect against

immediate hamstring MVC loss due to a greater ability to transmit the ground reaction forces laterally (from fibre to fibre) (Turrina *et al.*, 2013), which might disperse the force more efficiently to the tendon, while the muscle fibres themselves undergo less strain. Further, a greater BF_{LH} PCSA reflects more fibres aligned in parallel, which would be accompanied by more muscle connective tissue of the extracellular matrix, thus potentially protecting the muscle fibres from excessive damage during eccentric contractions.

The stem cells of the extracellular matrix also demonstrated an important role for muscle strength recovery in the subgroup of participants, as there was a strong inverse correlation between myoblast:fibroblast ratio and hamstring MVC torque recovery POST48. Skeletal muscles with an increased availability of fibroblasts around the area of myotrauma might have a better capacity to reorganise the complex extracellular matrix, thus restoring (lateral) force transmission, which results in a faster recovery of muscle strength after muscle damage. This was in line with the myoblast:fibroblast ratio effect on cellular aspects of muscle regeneration and remodelling assessed in primary muscle stem cells *in vitro*. Muscle stem cells with a low myoblast:fibroblast ratio revealed a faster wound closure (i.e. more cells migrated to the inner part of the artificial injury compared to the outer part), in particular 24 h after performing the scratch assay. However, this effect was less significant 48 h after the scratch protocol, and, at day seven, muscle primary cells with a higher myoblast:fibroblast ratio showed an improved myotube formation, which is in line with the investigation of Fry *et al.* (2014). Together, these results suggest that the abundance and activity of fibroblasts and myoblasts may play different roles, depending on the time points during muscle repair. A larger abundance of fibroblasts has a positive effect at the beginning of muscle repair, but a larger number of myoblasts is more important for the latter stage of muscle regeneration or hypertrophy, when myoblasts differentiate and fuse to become myotubes. We, therefore, assume that repeated maximal sprints with insufficient recovery of previously fatigued and damage muscles (where the fatigue and damage response is modulated by the muscle size and stem cell composition, respectively) might augment the risk of muscle strains, as appropriate damage to the muscle connective

352 tissue is thought to differentiate between exercise-induced muscle damage and muscle strains
353 (Valle *et al.*, 2017; Balius *et al.*, 2018).

354 ### Limitations

355 There was no relationship between the myoblast:fibroblast ratio and any physiological
356 variables regarding the quadriceps femoris, from which the muscle biopsies were obtained. It
357 has previously been shown that skeletal muscles of different origin, but with similar
358 physiological functions and fibre type composition, demonstrate similar transcriptome
359 expression patterns of up to 99% (Evangelidis *et al.*, 2016; Terry *et al.*, 2018). Therefore, the
360 correlation between myoblast:fibroblast ratio and the muscle damage-response of the
361 hamstrings but not the quadriceps muscles is likely explained by more severe ultrastructural
362 damage in the hamstrings than quadriceps. Furthermore, peripheral fatigue can be caused by
363 metabolic perturbations, such as the depletion of intramuscular glycogen (Howatson & Van
364 Someren, 2008). Therefore, because we did not control diet throughout the study, it is possible
365 that inter-individual differences in baseline muscle glycogen may have influenced the ability to
366 maintain maximal intensity throughout the sprints. However, participants were instructed to eat
367 and drink similar foods two hours before each laboratory visit, and to avoid strenuous exercise
368 for at least 48 h prior to the testing. Further, participants were given sufficient recovery between
369 sprint repetitions and there was a low decrement in sprint performance, indicating that
370 glycogen depletion was probably only a minor factor.

371 ## CONCLUSION

372 Repeated maximal sprints induces a greater and more prolonged strength loss in the
373 hamstrings compared to the quadriceps muscles. The immediate loss of hamstring function
374 appears to be due to both central (particularly reduced neuromuscular activation of the biceps
375 femoris long head) and peripheral fatigue, while prolonged hamstring strength loss is
376 predominantly linked to peripheral fatigue. Thigh neuromuscular fatigue following repeated
377 maximal sprints alters hip and knee kinematics during running immediately after the repeated

maximal sprints, but this (likely) protective effect is less evident 48 hours after the intervention, which may lead to an increased hamstring muscle injury risk. Furthermore, biceps femoris long head PCSA was inversely related to hamstring strength loss immediately after repeated maximal sprinting, suggesting that the structure of the muscle, including non-contractile tissue (e.g. the extracellular matrix) protects against neuromuscular fatigue. Skeletal muscles with an increased number of fibroblasts might have a better capacity to reorganise the complex extracellular matrix, which results in a faster recovery of muscle function after substantial muscle damage. However, a larger number of myoblasts seems to be more important for the latter stage of muscle regeneration. These novel findings improve our understanding of the physiological, biomechanical and cellular causes and effects of exercise-induced neuromuscular fatigue. The practical implications are that a 48 h recovery period following repeated maximal sprinting is insufficient, and might increase hamstring strain injury risk. Furthermore, increasing hamstring PCSA via resistance training is likely to reduce peripheral fatigue following repeated maximal sprinting, thereby reducing hamstring strain injury risk.

MATERIALS AND METHODS

Participants

In vivo repeated maximal sprint intervention: Twenty recreationally active and healthy young men (*mean* ± *SD*; age 20.3 ± 2.87 years; height 1.79 ± 0.05 m; body mass 75.0 ± 7.89 kg) participated in the repeated maximal sprint intervention.

In vitro muscle stem cell component: Eight healthy young male (age 21.25 ± 4.27 years; height 1.77 ± 0.05 m; body mass 73.78 ± 5.68 kg) and four healthy young female (age 25.5 ± 1.29 years; height 1.67 ± 0.08 m; body mass 61.40 ± 2.57 kg) participants provided a biopsy of the vastus lateralis muscle for the *in vitro* muscle stem cell component of this study. Six of the eight males also participated in the repeated maximal sprint intervention at least three weeks after providing a muscle biopsy. Only males were recruited for the repeated maximal sprint intervention, as there is some evidence of sex differences in neuromuscular fatigue (Wüst *et al.*, 2008). However, both men and women were recruited for the muscle stem cell component due to there being no reported sex differences in stem cell properties and none within our own pilot studies (data not shown). Prior to starting the study, written informed consent was obtained from each participant and pre-biopsy screening was performed by a physician for those participants who volunteered a muscle biopsy. The study was approved by the Research Ethics Committee of Liverpool John Moores University and complied with the Declaration of Helsinki. Volunteers were physically active but were ineligible to participate if they had performed strength training of the lower limbs within 6 months prior to participation in the study, which was determined during pre-participation screening. Further exclusion criteria were: (i) any lower limb injury in the past 12 months; (ii) age under 18 or above 35 years; and (iii) more than three structured exercise sessions per week.

Experimental Design of the Repeated Maximal Sprint Intervention *in vivo*

Participants were required to visit the temperature-controlled (22-24°C) laboratory on three occasions: (i) familiarisation, (ii) testing day including the PRE and POST assessments; and

(iii) POST48 assessments after the repeated maximal sprint intervention. One week prior to the testing day, participants were familiarised with the assessments as well as with repeated maximal sprints (by performing 2-3 submaximal sprints) and BF_{LH} architecture of the hamstring muscle group was assessed via ultrasound. On the test day, participants performed the repeated maximal sprint intervention of 15 x 30 m sprints to induce neuromuscular fatigue/damage in both the quadriceps femoris and hamstring muscle groups. All tests were performed at the same time of the day for each participant. Further, participants were instructed to maintain their normal routine (including eating habits), to refrain from drinking alcohol and to avoid any strenuous exercise 48 h prior to testing and throughout the study, and to refrain from consuming caffeine on testing days. Nothing was consumed throughout the testing sessions except water, which was available ad libitum.

The test battery was always performed in the same order with the right leg of each participant and comprised (i) venous blood sampling [for analysing serum interleukin-6 (IL-6) concentration and creatine kinase (CK) activity]; (ii) hamstrings and quadriceps muscle soreness via visual analogue scale; (iii) isometric maximum voluntary contraction (MVC) torque of the quadriceps, as well as both voluntary and involuntary muscle activation and torque-frequency relationship via electrical stimulation] MVC torque of the hamstring together with normalised BF_{LH} sEMG (see below); and (iv) treadmill running (4.17 m s^{-1}) kinematics of the right leg (via an eight-camera motion capture system) PRE and POST48 following the repeated maximal sprint intervention. At POST, kinematic assessments were performed first followed by the aforementioned order of the assessment for practical reasons.

Maximal Repeated Sprint Protocol

Many athletes in team sports are required to perform repeated maximal sprints, which are characterised by short-duration (<10 s) and relatively longer recovery times (>60 s) between maximal sprint bouts, and have a different physiological demand compared to repeated-sprint exercises with shorter recovery times (<60 s) (Bradley *et al.*, 2010; Girard *et al.*, 2011). Therefore, the IS intervention consisted of 15 repetitions of 30 m maximal sprints with a

445 deceleration zone of 12 m. The 30 m distance was chosen as the upper average of both the
446 total sprinting distance (346 ± 115 m) of wide-midfielders and the mean recovery time (70.2 ±
447 25.1 s) between sprint bouts in soccer (Bradley *et al.*, 2009; Bradley *et al.*, 2010), which allows
448 the athlete to maintain the performance of the sprint bouts. Similar protocols have been used
449 elsewhere (Timmins *et al.*, 2014; Verma *et al.*, 2015; Chen *et al.*, 2017). Prior to the repeated
450 maximal sprint intervention, a five-minute warm-up was performed, comprising jogging,
451 dynamic stretching and three self-paced 20 m runs at 60%, 80%, 100% of perceived top speed.
452 During the repeated maximal sprint intervention, the participants were instructed to sprint
453 maximally (verbal encouragement) and to stop within the deceleration zone. Further, they were
454 instructed to move slowly back to the start line and to sit on a chair for the remaining time until
455 the next sprint. The recovery comprised 90 s between repetitions and after every 5th repetition,
456 the participants were allowed to rest for 3 min. Sprinting time during trials was measured and
457 controlled with timing gates (Brower Timing Systems, Draper, UT, USA), which were placed
458 on the start and finish line. Participants started 30 cm before the start line to avoid interfering
459 with timing gates with the arms upon initial acceleration (Howatson & Milak, 2009). Further,
460 heart rate (Polar Oy, Kempele, Finland) and rating of perceived exertion (Borg, 1982) were
461 recorded before and after each repetition. Participants were instructed to wear the same
462 footwear for each testing day. As there was an upsurge in speed of the final sprint, fatigue was
463 assessed with the performance decrement score using the following formula (Glaister *et al.*,
464 2008):

465 $$Fatigue = \left(100\ X\ (total\ sprint\ time\ \div ideal\ sprint\ time)\right) - 100$$

466 Where total sprint time = sum of time from all 15 sprints; and ideal sprint time = total number
467 of sprints (15) x fastest repetition sprint time. The calculation of this decrement score was also
468 used to quantify changes in heart rate and rating of perceived exertion during the repeated
469 maximal sprint intervention.

Maximal Voluntary Contraction (MVC)

Three test sessions were conducted with an isokinetic dynamometer (Humac Norm, CSMI Solutions, Massachusetts, USA). As *isokinetic* maximum voluntary contractions (MVC) torque tests are only weak predictors of hamstring strain injury (van Dyk *et al.*, 2016), we decided to focus on *isometric* MVC quadriceps and hamstring torque at optimal knee strength angles (optimal torque-joint angle relationship, see below) to avoid further fatiguing the participants. The torque signal was interfaced with an acquisition system (AcqKnowledge, Biopac Systems, Santa Barbara, USA) for analogue-to-digital conversion and sampled at a frequency of 2 kHz. The participant was seated in an upright position and securely fastened with inextensible straps at the chest and waist while the arms were held crossed above the chest. The tibiofemoral epicondyle was aligned with the lever arm rotation axis, and the lever arm shin pad was strapped to the leg, 2 cm above the centre of the lateral malleolus. A Velcro strap secured the distal thigh just above the knee. The hip joint angle was set to 85° (180° = supine position) in order to analyse the knee flexor muscle group at a sprint specific angle associated with the late swing phase of sprinting (Guex *et al.*, 2012). Participants were instructed to maximally extend and flex their leg to measure knee range of motion. Quadriceps MVC was measured at 80º knee flexion (0º = full knee extension), as this is the optimal joint angle for peak quadriceps MVC in healthy young men (Erskine *et al.*, 2009). Hamstring MVC was measured at 30º knee flexion based on this being the optimal joint angle for peak hamstring MVC during our pilot work. Published studies during the time of data collection used a similar angle of hamstring MVC torque (Nedelec *et al.*, 2014; Kirk & Rice, 2016). This was also in line with sprinting kinematics, demonstrating that maximal hamstring muscle lengths during sprinting occur during the late swing phase when the knee is flexed between 30° and 45° (Thelen *et al.*, 2005). Prior to isometric MVC assessments, participants underwent a standardised warm up consisting of 10 submaximal isokinetic leg extensions ($60^{º}\cdot s^{-1}$). Participants then performed three isometric knee extension (quadriceps) and flexion (hamstring) at both joint angles (each MVC lasting 2-3 s), with 60 s rest between MVC of a given muscle group. The highest MVC of

the three attempts for each muscle group at each angle was used for subsequent analyses. Throughout the tests, participants received verbal encouragement and biofeedback (MVC outputs) were projected onto a screen in front of the participant.

Hamstring Muscle Voluntary Activation

To measure hamstring muscle voluntary activation capacity via the interpolated twitch technique, stimulation electrodes (12.5 mm x 7.5 mm self-adhesive electrodes (DJO Global, California, USA) were used. The general procedure has been described elsewhere (Erskine *et al.*, 2009; Erskine *et al.*, 2010; Marshall *et al.*, 2014). Briefly, the anode was placed proximal to the popliteal fossa, and the cathode was placed beneath the gluteal fold and slightly medial to avoid activation of the vastus lateralis. Protocols were completed with electrical stimulation pads carefully taped down during the sprinting protocol and were additionally marked on the skin with a permanent marker, to ensure a precise relocation for the POST and POST48 tests. Stimulation was delivered by a high-voltage stimulator (DS7AH; Digitimer Ltd., Welwyn Garden City, United Kingdom), and consisted of a doublet using two 240-V rectangular pulses (200 μs pulse width) with an inter-pulse duration of 10 ms (100 Hz stimulation). During each experimental session, relaxed hamstring muscles were stimulated while participants were fixed in the isokinetic dynamometer with the same setting for knee flexion MVC (85º hip angle, 30 º knee flexion). The amplitude started with 50 mA to familiarise the participants to the stimulation and was gradually increased in 20 mA increments until a plateau in doublet torque was achieved. We decided to use the individual maximal stimulation (100 %) intensity despite the fact that other publications used supramaximal stimulation (110-130 %) (Marshall *et al.*, 2014) as we experienced lower MVC knee flexion torque output beyond 100 %. That individual amplitude (162.0 ± 17.4 mA; range: 130–200 mA) was applied during all maximal contractions in the experimental session.

The maximal doublet stimulation was used two minutes later to elicit resting maximal doublet torque in the resting state (control doublet), followed 2.5 s later by a second (superimposed) doublet during an isometric knee flexion MVC. The superimposed doublet torque was always

524 calculated manually from careful selection and inspection of the respective time periods
525 compared to a normal increase in voluntary torque. Voluntary activation was calculated
526 according to the following equation:

527 $$VA\ (\%) = [1 - (superimposed\ doublet\ torque / control\ doublet\ torque)]$$

528 **Surface Electromyography and Antagonist Muscle Co-activation**

529 Surface electromyographic (sEMG) activity was recorded from the vastus lateralis and BF_{LH} to
530 determine the extent of antagonist muscle co-activation during MVCs of the respective muscle
531 group. Previous reports have shown that the vastus lateralis (Reeves *et al.*, 2004) and BF_{LH}
532 (Kellis & Baltzopoulos, 1999) are representative muscles for the quadriceps femoris and
533 hamstring muscle group, respectively. This procedure has been reported in detail elsewhere
534 (Reeves *et al.*, 2004). Briefly, once the muscles were identified via palpation, and the skin
535 surface was shaved and cleaned with 70% ethanol, two bipolar Ag-AgCl surface electrodes
536 with an inter-electrode distance of 2 cm (Noraxon duel sEMG electrode, Noraxon, Scottsdale,
537 USA) were placed along the sagittal axis over the muscle belly at 33% of the respective muscle
538 length from the distal end [according to SENIAM guidelines (Hermens *et al.*, 2000)] and one
539 reference electrode (Ambu Blue, Ambu, Copenhagen, Denmark) was positioned over the
540 medial tibial condyle. The exact location of the electrodes were marked on the participant's
541 skin with a permanent marker to ensure precise electrode repositioning for the following
542 assessments.

543 Surface EMG signals were sampled at 2000 Hz (Biopac Systems, Santa Barbara, USA) and
544 then band-pass filtered between 10–500 Hz (AcqKnowledge, Biopac Systems, Santa Barbara,
545 USA). Surface EMG activity of both the agonist and antagonist muscles were analysed by
546 calculating the root mean square of the sEMG signal of a 500-ms epoch around peak MVC.
547 To compare BF_{LH} sEMG activity at all three time points, BF_{LH} sEMG of the hamstring MVC at
548 30° was normalised to the evoked maximum compound muscle action potential (M-wave) of
549 the BF_{LH} (see below). Antagonist muscle co-activation (i.e. quadriceps activation during

hamstring MVC at 30° knee flexion, or hamstring activation during quadriceps MVC at 80° knee flexion) was calculated with the following formula (where EMG_{max} is the maximum sEMG of the antagonist muscle when acting as an agonist at the same knee joint angle):

$$Antagonist\ muscle\ co-activation = \frac{EMGantagonist}{EMGmax} \times 100$$

Torque signals, electrical stimuli, and sEMG activity were displayed on a computer screen, interfaced with an acquisition system (AcqKnowledge, Biopac Systems, Santa Barbara, USA) used for analogue-to-digital conversion. Due to technical issues, co-activation data were available for hamstring n = 12; and quadriceps n=10.

Hamstring Muscle Maximal Compound Muscle Action Potential

The hamstring muscle group was stimulated with single square wave twitch pulses (200 µs duration) using the same electrical stimulator and stimulating electrodes, as described above. While the participant sat resting on the isokinetic dynamometer with the knee angle set at 30° knee flexion, compound muscle action potentials (*M*-waves) were evoked with 10 to 20 mA incremental amplitudes until a maximal *M*-wave (M_{max}) was achieved. The average amplitude necessary to evoke a maximal *M*-wave was 166.8 ± 19.8 mA; range: 130–210 mA). The maximal *M*-wave was defined as the mean peak-to-peak sEMG response from the three highest observed *M*-waves. Due to inter-individual differences in subcutaneous fat and the (re)location of small sEMG electrodes over a relatively large muscle belly, sEMG amplitude is notoriously variable (Araujo *et al.*, 2000). To reduce this inter- and intra-individual variability, we normalised absolute BF_{LH} sEMG to the individual's BF_{LH} maximal *M*-wave, determined at each testing session (Lanza *et al.*, 2018). Due to technical issues, data of BF_{LH} sEMG normalised to maximal *M*-wave was only available for n = 13.

Torque-frequency Relationship

The torque-frequency relationship was determined by stimulating the hamstring muscle group with single square wave twitch pulses (200 µs duration) at 1, 10, 15, 20, 30, 50 and 100 Hz for

1 s each in a random order and with 15 s rest between each stimulation, using the same electrical stimulator and stimulating electrodes (and location), as described above. The stimulus intensity for 100-Hz stimulation was the amplitude necessary to elicit ~20 % knee flexion MVC torque at PRE, and the same amplitude was used for the same test at POST and 48POST. The absolute peak torque at each frequency was normalised to the peak torque at 100 Hz for each time point (PRE, POST and POST48).

Delayed Onset Muscle Soreness

Using a visual analogue scale that consisted of a 100 mm line (scale 0-10 cm; 0 cm=no soreness; 10 cm= unbearably painful), in conjunction with both a three-repetition bilateral squat (predominantly to determine quadriceps femoris muscle soreness) (Scott & Huskisson, 1979) and lunges (predominantly to determine hamstring muscle soreness), participants rated their perceived lower limb muscle soreness along the muscle length immediately after each movement. Muscle soreness was also measured by recording the force required to elicit tenderness at nine fixed sites on the skin over the quadriceps (distal, central and proximal locations of the three superficial quadriceps heads, vastus lateralis, vastus medialis and rectus femoris) and six sites on the hamstrings (distal, central and proximal locations of both BF_{LH} and the medial hamstrings), which were previously marked with a permanent marker to ensure the same measuring position PRE, POST and POST48. At each site, a gradually increasing force was applied by the investigator with an algometer (FPK/FPN Mechanical Algometer, Wagner Instruments, Greenwich, USA) with a maximum of 10 kg/cm^2. Lying in the prone position with the hip and knee fully extended and muscles relaxed, the participant was asked to indicate when the sensation of pressure changed to discomfort, and the force at that point was recorded (Newham *et al.*, 1987).

Ultrasound

Architectural parameters of the BF_{LH} were assessed using B-mode ultrasound imaging. Participants were in the prone position with the hip and knee fully extended and muscles

relaxed. The BF_{LH} was investigated, as this muscle is the most commonly injured hamstring muscle in team sports, particularly during sprinting (Ekstrand *et al.*, 2011). Longitudinal and cross-sectional panoramic ultrasound images of the right BF_{LH} were obtained (Philips EPIQ 7 Ultrasound System, Bothel, USA). The linear transducer (5-18 MHz; aperture 38.9 mm) was carefully placed on the skin with transmission gel and BF_{LH} was scanned (i) longitudinally from its distal (=0% muscle length) to proximal (=100% muscle length) myotendinous junction along a line drawn with a permanent marker to mark the central pathway between the medial and lateral aspects of the muscle (incorporating the intra-muscular aponeurosis (Evangelidis *et al.*, 2014) (Figure 2A); and (ii) cross-sectionally at 20, 40, 60 and 80% along the total muscle length, measured on the skin using a tape measure (Seca, Hamburg, Germany) (Figure 2B).

All images were analysed offline (ImageJ, version 1.51s, National Institutes of Health, Bethesda, USA). Two images for each of the four cross-sectional points were recorded and the image of best quality was used to calculate BF_{LH} muscle volume. The volume of the muscular portion between every two consecutive scans was calculated with the following equation:

$$Volume = \frac{1}{3} * d * \left(a + \sqrt{(ab) + b}\right)$$

Where *a* and *b* are the anatomical cross-sectional areas of the muscle of two consecutive cross-sectional scans and *d* is the interval distance between the cross-sectional area measurements. The volume of the entire muscle was calculated by summing up all of the inter-scan muscular volumes (Erskine *et al.*, 2016). Two full-length sagittal images were then recorded to allow for the measurement of resting BF_{LH} muscle fascicle length and pennation angle, which were both assessed in 3 fascicles at 50 % of the total length of BF_{LH}. This point was measured offline (ImageJ). A comparison between offline (sagittal ultrasound) and tape measurements of the total BF_{LH} length revealed a very high correlation (R^2=0.958, P<0.001). Fascicle length was measured by tracing the fascicular path from the upper aponeurosis to the intra-muscular aponeurosis of the BF_{LH}. Muscle fascicle pennation angle was determined as

the angle between the muscle fascicular paths and their insertion into the intra-muscular aponeurosis. The mean of the three measurements for each parameter were used to determine both fascicle length and pennation angle of the BF_{LH} muscle. PCSA was calculated by dividing BF_{LH} volume by its fascicle length. During the time of data collection, a similar methodological approach was published elsewhere (Seymore *et al.*, 2017). One longitudinal image of one participant in the present study was not analysed due to low image quality. Ultrasound scans and image analysis was performed by the same investigator.

Kinematic and Kinetic Data

Three-dimensional kinematic and kinetic data were synchronously collected at 500 Hz using an eight-camera motion analysis system (Qqus 300+; Qualisys, Gothenburg, Sweden), together with a ground-embedded force plate (90 x 60 cm, 9287B; Kistler Holding, Winterthur, Switzerland) at 1,500 Hz. The data were filtered with a digital dual low-pass Butterworth filter at 20 Hz for motion and 60 Hz for force, as previously described (Verheul *et al.*, 2017). Retroreflective markers (12 mm diameter) were placed on anatomical landmarks on the right leg and pelvis, as previously described (McClay & Manal, 1999). One standing static and two functional motion calibration trials were recorded of the participant PRE, POST and POST48. For the static trial, participants stood with their feet approximately shoulder width apart and knees fully extended. This static trial determined local coordinate systems, the location of joint centres, and the foot, shank, thigh, and pelvis segment lengths of each participant. The functional trials defined functional hip joint centres (Schwartz & Rozumalski, 2005) and knee joint axes (Robinson & Vanrenterghem, 2012). Kinematic data were tracked using Qualisys Track Manager Software (Qualisys). Data processing and analysis were undertaken in Visual3D (C-Motion, Germantown, MD). To examine any changes between the time points, joint angles were normalised relative to the static trial of the accompanying time point for minimising the influence of potential slightly different marker positions between the trials. Lower extremity 3D joint angles and angular velocities were calculated using an X-Y-Z Cardan angle rotation sequence. Investigated variables included peak knee and hip angles, as well as

range of motion and time during stance and swing phase of the treadmill run, for all three planes, were calculated as described in previous studies (Verheul *et al.*, 2017).

Motorised Treadmill Run

Participants ran on a motorised treadmill (HP Cosmos Pulsar; Nussdorf, Germany) for 30 s at 4.17 m s^{-1} (0° incline), as high-speed running was of interest. The selected speed was based on pilot testing, which demonstrated that 15 km/h was the fastest speed on a motorized treadmill where the participants still felt comfortable. Motion analysis data were recorded for the last 10 s of the run and data were analysed for at least 6 consecutive strides. Peak knee and hip angle data, for all three planes, were calculated (i) between the initial contact and terminal stance of foot; and (ii) between initial and terminal swing phase. The touchdown of the foot during the treadmill run was determined from the kinematic data as occurring at the local minima and the toe-off during running as the local maxima of the vertical velocity of the head of the fifth metatarsal marker on the foot (Maiwald *et al.*, 2009).

Blood Samples

A 10 mL blood sample was drawn from an antecubital vein in the forearm and collected into a serum vacutainer (BD Vacutainer systems, Plymouth, UK). The blood samples were obtained at each time point and left at 22-24°C for 30 min to allow clotting, and then kept on ice when necessary. Serum samples were centrifuged at 1,300 g for 15 min at 4°C. All samples were then aliquoted into 1.5 mL microcentrifuge tubes [Axygen (Corning), New York, USA] and stored at -80°C until subsequent analysis (see below).

Serum Interleukin-6 (IL-6) Concentration

Serum samples were assayed for IL-6 concentration using commercially available human IL-6 enzyme linked immunosorbent assay kits (Quantikine®, R&D systems, Minneapolis, MN, USA) according to the manufacturer's instructions. The intensity of the colour produced after 20 min was measured with a Thermo Multiskan Spectrum microplate reader (Thermo Fisher

679 Scientific. Waltham, MA. USA) at 450 nm and values were calculated with Excel 365 (Microsoft,
680 v. 365, USA) by generating a four-parameter logistic curve fit. The minimum detectable dose
681 of human IL-6 was 0.70 pg/mL.

682 **Serum Creatine Kinase Activity**

683 Creatine kinase (CK) activity was assayed using a commercially available CK assay
684 (Catachem Inc., Connecticut, NE, USA), as described in detail elsewhere (Owens *et al.*, 2015).
685 Briefly, 10 µL blood serum were loaded onto a 96-well UV plate. The CK reaction reagent and
686 diluent (Catachem) were prepared as per the manufacturer's instructions and added to the
687 samples and the change in absorbance monitored continuously over 20 min in a Thermo
688 Multiskan Spectrum plate reader (Thermo Fisher Scientific. Waltham, MA. USA) at a
689 wavelength of 340 nm.

690 **Capillary Blood Lactate Concentration**

691 Capillary blood samples were taken from the finger-tip via a Safety-Lancet Extra 18G needle
692 (Sarstedt; Nümbrecht, Germany) at rest before and immediately after the repeated maximal
693 sprint intervention. Blood samples were analysed within 60 seconds of collection using a
694 portable blood lactate analyser (Arkray Lactate Pro; Kyoto, Japan).

695 **Reagents, Chemicals, and Solvents for Muscle Cell Culture *in vitro***

696 Growth media used for the expansion of human muscle-derived cell populations consisted of
697 Hams F-10 nutrient mix (Lonza, Basel, Switzerland) with added L-glutamine (2.5 mM), 10%
698 heat-inactivated fetal bovine serum (hiFBS; Gibco, Thermo Fisher Scientific, Altincham, UK),
699 1% penicillin-streptomycin (Life Technologies, Warrington, UK), and 1% L-Glutamine (Gibco).
700 Differentiation media consisted of α-MEM (Lonza), 1% hiFBS, 1% penicillin-streptomycin, and
701 1% L-glutamine. Phosphate-buffered saline (PBS; Sigma-Aldrich) was used to wash cell
702 monolayers. Desmin polyclonal rabbit anti-human antibody (Cat# ab15200, RRID: AB_301744)
703 was used (1:200) from Abcam (Abcam, Cambridge, UK), and secondary antibody (TRITC

polyclonal goat anti-rabbit; Cat# A16101, RRID: AB_2534775) was used (1:200) from Fisher Scientific.

Muscle Biopsy Procedure

Participants were instructed to avoid any strenuous exercise 48 h prior to the biopsy procedure. Biopsies from the vastus lateralis muscle were obtained under local anaesthesia from each participant, using the Weil-Blakesley conchotome technique as described previously (Baczynska *et al.*, 2016). The conchotome was inserted through the incision into the muscle belly to obtain the 134 ± 82.7 mg muscle biopsy.

Extraction of Human Muscle-Derived Cells

The muscle biopsies analysed in this study were isolated (Blau & Webster, 1981; Crown *et al.*, 2000) and cultured (Owens *et al.*, 2015), as reported previously. Briefly, biopsy samples were transferred with precooled growth media from the muscle biopsy suite to the sterile tissue culture hood (Kojair Biowizard Silverline class II hood; Kojair, Vippula, Finland) within 40 min and muscle biopsy samples were washed three times with ice-cold PBS (0.01 M phosphate buffer, 0.0027 M KCl, and 0.137 M NaCl, pH 7.4, in dH2O). Visible fibrous and fat tissue was removed using sterile scissor and forceps. Samples were cut in small pieces (1 mm^3) and digested in 5 ml of trypsin-EDTA for 15 min on a magnetic stirring platform at 37°C to dissociate muscle cells. The trypsinisation process was repeated twice. Supernatant derived following each treatment was collected and pooled with hiFBS at a concentration of 10% of the total volume to inhibit further protease activity. Cell supernatant was centrifuged at 450 g for 5 min. Supernatant was discarded and the cell pellet was resuspended in growth media and plated on a T25 cm^2 culture flask (Corning, Life Sciences, New York, USA) for cell population expansion. Culture flasks were previously coated with a 2 mg/l porcine gelatin solution (90–110 g, Bloom; Sigma-Aldrich, Dorset, UK) to support cell adhesion.

Expansion of Extracted Cells

The medium was refreshed on the fourth day after the extraction procedure and subsequently every 48 h following two brief washes with PBS. Cells were incubated in a HERAcell 150i CO_2 Incubator (Thermo Scientific, Cheshire, UK). T25 cm^2 culture flasks reached 80% confluence after aproximately 10 days and were passaged via trypsinisation. Cells were counted using Trypan Blue exclusion and re-plated on gelatinised T75 cm^2 culture flasks (Nunc, Roskilde, Denmark). The cells were expanded until passage 3 and then frozen in GM with 10% dimethyl sulfoxide (DMSO) in liquid N_2 as a cryopreservant. All experiments were performed on cells between passages 3 and 6 to avoid potential issues of senescence (Foulstone *et al.*, 2004).

Characterization of Human Muscle-Derived Cells

The mixed population of human skeletal muscle-derived myoblasts and fibroblasts were characterised by immunofluorescent staining for the detection of desmin expressed by myoblasts (desmin positive) and non-myoblasts (desmin negative) to determine the percentage of myoblasts and fibroblasts. Previous investigations have determined that the non-myoblast (desmin negative) fraction is highly enriched in fibroblasts, with up to 99 % of this fraction being fibroblasts (Stewart *et al.*, 2003; Agley *et al.*, 2013). Therefore, non-myoblasts (desmin negative) were referred to here as fibroblasts.

Grohmann *et al.* (2005) showed that passaging does not change the percentage of myoblast and fibroblasts and all populations were included for analysis. Monolayers were incubated with 25% [vol/vol methanol in Tris-buffered saline (10 mmTris-HCl, pH 7.8, 150 mm NaCl)], 50% and 100% for 5-min to fix the cells and stored at 4°C wet in Tris-buffered saline until further analysis. Fixed monolayers were permeabilised and blocked for 2 h with 5% goat serum and 0.2% Triton X-100 in Tris-buffered saline, prior to staining. Cells were incubated overnight at 4°C with anti-Desmin antibody (1:200). After overnight incubation, the primary antibody was removed, and the cells were washed three times with Tris-buffered saline. Secondary TRITC polyclonal goat anti-rabbit antibody (1:200) was then applied and incubated for 2 h at 4°C.

Fluorescent images were captured using live imaging microscopy (Leica DMB 6000; Magnification x 10.5) and analysed via ImageJ cell counter plug-in. A total of four randomly selected areas per well were analysed per individual.

Wound-Healing Assay, Migration and Differentiation Analysis

For the wound healing assay, 100,000 cells/ml were seeded in gelatinised six-well plates (Nunc, Roskilde, Denmark). Cells were expanded as described above until cell monolayers reached a confluent state, Growth media was removed, monolayers were washed with PBS and cells were damaged by a vertical scrape with a 1-ml pipette tip (width of the wound area, *mean* ± *S.E.M.*: 896.4 ± 21.24 *μ*m), as previously reported by our group (Owens *et al.*, 2015; Brown *et al.*, 2017). PBS was aspirated, damaged cell monolayers were washed twice with PBS to remove cell debris and 2 ml differentiation media was added. Monolayers were imaged with a live imaging microscopy (Leica) for the analysis of cell migration immediately, 24h, 48h and seven days after the wound healing assay. Additional 500 µl differentiation media was added in each well at day 4. TIF images were exported from Leica Application Suite and loaded as TIF image stacks in ImageJ with a cell counter plug-in. Cells in the outer and inner segments were then counted (Figure 4A).

Damaged monolayers were imaged at two sites per well in the wound site immediately post-damage (0 h). These image coordinates were tracked and stored to allow subsequent monitoring of the same sites on the wound to reduce this experimental bias. Myotube formation was captured on day 7. Captured images were exported as TIF image files, and analysed in ImageJ. Muscle cell fusion/differentiation was assessed as the number of myotubes per field of view and myotube hypertrophy was determined by measuring myotube length, myotube diameter (the average of three diameters along the length of the myotube), myotube area (determined by manually drawing a line around the sarcolemma of each myotube) and total myotube number via ImageJ cell counter plug-in. By normalising the pixel scale to the micron scale of each image, a value expressed as μm^2 was obtained for myotube area. A total of two images per well were analysed.

Creatine Kinase (CK) Activity

At 0 and 10 days following the mechanical scrape insult, CK activity was analysed as a marker of muscle cell differentiation/fusion into myotubes. Cell monolayers were first lysed with 300 µl/well of 50 M Tris-mes and 1% Triton-X 100, pH 7.8 (TMT). Ten microliters of TMT cell lysate was loaded in duplicate wells on a 96-well UV plate and used for quantification of CK activity. The CK reaction reagent and diluent (Catachem, Bridgeport, CT, USA) were prepared as per the manufacturer's instructions as previously described (please see subsection Serum Creatine Kinase).

Statistical Analysis

One-way repeated-measures analysis of variances (ANOVA)s were performed to determine whether there was a significant main effect for time (within subject factor) for the following dependent variables: MVC torque, voluntary muscle activation, antagonist muscle co-activation, muscle soreness (for squat lunge via measured via visual analogue scale as well as algometer), rating of perceived exertion, CK activity, IL-6 concentration, and for kinematics data (hip and knee angle parameters). MVC torque data were analysed for interactions and main effects for muscle group and time using two-way mixed design ANOVAs, comparing differences between muscle groups across 3-time points; PRE, POST, and POST48. For within test comparisons, either, independent t-tests, or one-way ANOVAs were used where appropriate. For the torque-frequency relationship, normalised torque at each frequency was analysed using a two-way repeated measures ANOVA, with stimulation frequency (1-100 Hz) and time (PRE, POST and POST48) as the within-groups independent variables. Post-hoc one-way repeated measures ANOVAs were used to determine if the normalised torque at each frequency differed between time points. Bivariate correlations were used to analyse the relation between architectural parameters of the BF_{LH} (volume, fascicle length, fascicle pennation angle and PCSA) and fatigue biomarkers (relative MVC loss normalised to PRE MVC), serum CK activity, serum IL-6 concentration, muscle soreness, knee joint range of motion or changes in range of motion during treadmill running.

Bivariate correlations were used to analyse the relation between myoblast:fibroblast ratio and quadriceps and hamstring MVC, migration dynamics (total cell migration, cell proportion of inner to outer segment) and myotube formation (total myotube number, myotube length, average diameter, myotube area and CK activity) of the muscle stem cells. Standard guidelines concerning violation of the sphericity assumption to adjust the degree of freedom of the F-test by the Huynh-Felt epsilon if epsilon is greater than 0.75 and to use the more stringent Greenhouse-Geisser adjustment if epsilon is less than 0.75 were followed. Results were expressed as mean ± SD, unless otherwise stated, with statistical significance set at $P<0.05$. All MVC data were analysed with AcqKnowledge software 4.4 (Biopac-Systems Inc., Goleta, USA) and SPSS 23 Software (IBM Inc., Armonk, NY: IBM Corp) was used for statistical analysis. Occasional missing data are reflected in the reported degrees of freedom.

GRANTS

This study was supported by a Liverpool John Moores University PhD studentship (P.B.) and the Wellcome Trust Biomedical Vacation Scholarships (R.M.E., M.S.).

DISCLOSURES

No conflicts of interest, financial or otherwise, are declared by the authors.

AUTHOR CONTRIBUTION

R.M.E, P.B., B.D., C.E.S., and M.L. conceived and designed the research; P.B., S.T., M.S., M.C., J.A.S., and S.O.S performed the experiments; P.B., S.T. and R.M.E analyzed the data; R.M.E., P.B, M.L. and C.E.S. interpreted the results of the experiments; P.B. prepared the figures; P.B. drafted the manuscript; R.M.E., P.B., S.T., M.S., M.L., B.D., C.E.S., M.C., J.A.S., and S.O.S edited and approved the final version of the manuscript.

REFERENCES

Agley CC, Rowlerson AM, Velloso CP, Lazarus NR & Harridge SD. (2013). Human skeletal muscle fibroblasts, but not myogenic cells, readily undergo adipogenic differentiation. *Journal of cell science*, jcs. 132563.

836 Araujo RC, Duarte M & Amadio AC. (2000). On the inter-and intra-subject variability of the
837 electromyographic signal in isometric contractions. *Electromyogr Clin Neurophysiol* **40,** 225-
838 230.
839
840 Baczynska AM, Shaw S, Roberts HC, Cooper C, Sayer AA & Patel HP. (2016). Human Vastus Lateralis
841 Skeletal Muscle Biopsy Using the Weil-Blakesley Conchotome. *Journal of Visualized*
842 *Experiments***,** e53075-e53075.
843
844 Balius R, Alomar X, Pedret C, Blasi M, Rodas G, Pruna R, Peña-Amaro J & Fernández-Jaén T. (2018).
845 Role of the Extracellular Matrix in Muscle Injuries: Histoarchitectural Considerations for
846 Muscle Injuries. *Orthopaedic Journal of Sports Medicine* **6,** 2325967118795863.
847
848 Balsom P, Seger J, Sjödin B & Ekblom B. (1992). Maximal-intensity intermittent exercise: effect of
849 recovery duration. *Int J Sports Med* **13,** 528-528.
850
851 Blau HM & Webster C. (1981). Isolation and characterization of human muscle cells. *Proc Natl Acad*
852 *Sci* **78,** 5623-5627.
853
854 Borg GA. (1982). Psychophysical bases of perceived exertion. *Medicine and science in sports and*
855 *exercise* **14,** 377-381.
856
857 Bradley PS, Di Mascio M, Peart D, Olsen P & Sheldon B. (2010). High-intensity activity profiles of elite
858 soccer players at different performance levels. *J Strength Cond* **24,** 2343-2351.
859
860 Bradley PS, Sheldon W, Wooster B, Olsen P, Boanas P & Krustrup P. (2009). High-intensity running in
861 English FA Premier League soccer matches. *Journal of sports sciences* **27,** 159-168.
862
863 Brown AD, Close GL, Sharples AP & Stewart CE. (2017). Murine myoblast migration: influence of
864 replicative ageing and nutrition. *Biogerontology* **18,** 947-964.
865
866 Byrne C, Twist C & Eston R. (2004). Neuromuscular function after exercise-induced muscle damage.
867 *Sports Med* **34,** 49-69.
868
869 Chen C-H, Ye X, Wang Y-T, Chen Y-S & Tseng W-C. (2017). Differential Effects of Different Warm-up
870 Protocols on Repeated Sprints-Induced Muscle Damage. *J Strength Cond*.
871
872 Chumanov ES, Schache AG, Heiderscheit BC & Thelen DG. (2012). Hamstrings are most susceptible to
873 injury during the late swing phase of sprinting. *Br J Sports Med* **46,** 90.
874
875 Crema MD, Jarraya M, Engebretsen L, Roemer FW, Hayashi D, Domingues R, Skaf AY & Guermazi A.
876 (2017). Imaging-detected acute muscle injuries in athletes participating in the Rio de Janeiro
877 2016 Summer Olympic Games. *Br J Sports Med***,** bjsports-2017-098247.
878
879 Crown A, He X, Holly J, Lightman S & Stewart C. (2000). Characterisation of the IGF system in a
880 primary adult human skeletal muscle cell model, and comparison of the effects of insulin and
881 IGF-I on protein metabolism. *J Endocrinol* **167,** 403-415.
882
883 Ekstrand J, Hägglund M & Waldén M. (2011). Epidemiology of muscle injuries in professional football
884 (soccer). *The American journal of sports medicine* **39,** 1226-1232.
885

Erskine R, Tomlinson D, Morse C, Winwood K, Hampson P, Lord J & Onambélé G. (2016). The individual and combined effects of obesity-and ageing-induced systemic inflammation on human skeletal muscle properties. *Int J Obes (Lond)*.

Erskine RM, Jones DA, Maganaris CN & Degens H. (2009). In vivo specific tension of the human quadriceps femoris muscle. *Eur J Appl Physiol* **106,** 827-838.

Erskine RM, Jones DA, Williams AG, Stewart CE & Degens H. (2010). Resistance training increases in vivo quadriceps femoris muscle specific tension in young men. *Acta physiologica* **199,** 83-89.

Evangelidis P, Massey GJ, Ferguson RA, Wheeler PC, Pain MT & Folland JP. (2016). The functional significance of hamstrings composition: is it really a 'fast'muscle group? *Scandinavian journal of medicine & science in sports* **27,** 1181-1189.

Evangelidis PE, Massey GJ, Pain M & Folland JP. (2014). Biceps Femoris Aponeurosis Size: A Potential Risk Factor for Strain Injury? *Medicine and science in sports and exercise*.

Foulstone EJ, Huser C, Crown AL, Holly JM & Stewart CE. (2004). Differential signalling mechanisms predisposing primary human skeletal muscle cells to altered proliferation and differentiation: roles of IGF-I and TNFα. *Experimental cell research* **294,** 223-235.

Franchi MV & Maffiuletti NA. (2019). Distinct modalities of eccentric exercise: different recipes, not the same dish. *J Appl Physiol* **0,** null.

Friden J, Sjöström M & Ekblom B. (1983). Myofibrillar damage following intense eccentric exercise in man. *Int J Sports Med* **4,** 170-176.

Fry CS, Kirby TJ, Kosmac K, McCarthy JJ & Peterson CA. (2017). Myogenic progenitor cells control extracellular matrix production by fibroblasts during skeletal muscle hypertrophy. *Cell stem cell* **20,** 56-69.

Fry CS, Lee JD, Jackson JR, Kirby TJ, Stasko SA, Liu H, Dupont-Versteegden EE, McCarthy JJ & Peterson CA. (2014). Regulation of the muscle fiber microenvironment by activated satellite cells during hypertrophy. *FASEB J* **28,** 1654-1665.

Gillies AR & Lieber RL. (2011). Structure and function of the skeletal muscle extracellular matrix. *Muscle Nerve* **44,** 318-331.

Girard O, Mendez-Villanueva A & Bishop D. (2011). Repeated-Sprint Ability—Part I. *Sports Med* **41,** 673-694.

Glaister M, Howatson G, Pattison JR & McInnes G. (2008). The reliability and validity of fatigue measures during multiple-sprint work: an issue revisited. *J Strength Cond* **22,** 1597-1601.

Grohmann M, Foulstone E, Welsh G, Holly J, Shield J, Crowne E & Stewart C. (2005). Isolation and validation of human prepubertal skeletal muscle cells: maturation and metabolic effects of IGF-I, IGFBP-3 and TNFα. *J Physiol* **568,** 229-242.

Guex K, Gojanovic B & Millet GP. (2012). Influence of hip-flexion angle on hamstrings isokinetic activity in sprinters. *Journal of athletic training* **47,** 390-395.

Hermens HJ, Freriks B, Disselhorst-Klug C & Rau G. (2000). Development of recommendations for SEMG sensors and sensor placement procedures. *Journal of electromyography and Kinesiology* **10,** 361-374.

Howatson G & Milak A. (2009). Exercise-induced muscle damage following a bout of sport specific repeated sprints. *J Strength Cond* **23,** 2419-2424.

Howatson G & Van Someren KA. (2008). The prevention and treatment of exercise-induced muscle damage. *Sports Med* **38,** 483-503.

Joe AW, Yi L, Natarajan A, Le Grand F, So L, Wang J, Rudnicki MA & Rossi FM. (2010). Muscle injury activates resident fibro/adipogenic progenitors that facilitate myogenesis. *Nat Cell Biol* **12,** 153.

Jones D, Newham D, Round J & Tolfree S. (1986). Experimental human muscle damage: morphological changes in relation to other indices of damage. *J Physiol* **375,** 435-448.

Jonhagen S, Nemeth G & Eriksson E. (1994). Hamstring injuries in sprinters the role of concentric and eccentric hamstring muscle strength and flexibility. *The American Journal of Sports Medicine* **22,** 262-266.

Kellis E & Baltzopoulos V. (1999). In vivo determination of the patella tendon and hamstrings moment arms in adult males using videofluoroscopy during submaximal knee extension and flexion. *Clinical Biomechanics* **14,** 118-124.

Kirk EA & Rice CL. (2016). Contractile function and motor unit firing rates of the human hamstrings. *J Neurophysiol***,** jn. 00620.02016.

Lanza MB, Balshaw TG, Massey GJ & Folland JP. (2018). Does normalization of voluntary EMG amplitude to MMAX account for the influence of electrode location and adiposity? *Scand J Med Sci Sports*.

Mackey AL, Magnan M, Chazaud B & Kjaer M. (2017). Human skeletal muscle fibroblasts stimulate in vitro myogenesis and in vivo muscle regeneration. *J Physiol* **595,** 5115-5127.

Maiwald C, Sterzing T, Mayer T & Milani T. (2009). Detecting foot-to-ground contact from kinematic data in running. *Footwear Science* **1,** 111-118.

Marshall PW, Lovell R, Jeppesen GK, Andersen K & Siegler JC. (2014). Hamstring muscle fatigue and central motor output during a simulated soccer match. *PLoS One* **10,** e102753.

McClay I & Manal K. (1999). Three-dimensional kinetic analysis of running: significance of secondary planes of motion. *Medicine and Science in Sports and Exercise* **31,** 1629-1637.

Murphy MM, Lawson JA, Mathew SJ, Hutcheson DA & Kardon G. (2011). Satellite cells, connective tissue fibroblasts and their interactions are crucial for muscle regeneration. *Development* **138,** 3625-3637.

Nedelec M, McCall A, Carling C, Legall F, Berthoin S & Dupont G. (2014). The influence of soccer playing actions on the recovery kinetics after a soccer match. *J Strength Cond* **28,** 1517-1523.

Newham D, Jones D & Clarkson P. (1987). Repeated high-force eccentric exercise: effects on muscle pain and damage. *J Appl Physiol* **63,** 1381-1386.

Newham D, McPhail G, Mills K & Edwards R. (1983). Ultrastructural changes after concentric and eccentric contractions of human muscle. *J Neurol Sci* **61,** 109-122.

Onishi H, Yagi R, Oyama M, Akasaka K, Ihashi K & Handa Y. (2002). EMG-angle relationship of the hamstring muscles during maximum knee flexion. *Journal of Electromyography and Kinesiology* **12,** 399-406.

Opar DA, Williams M, Timmins R, Hickey J, Duhig S & Shield A. (2014). Eccentric hamstring strength and hamstring injury risk in Australian footballers. *Medicine & Science in Sports & Exercise* **46**.

Opar DA, Williams MD & Shield AJ. (2012). Hamstring strain injuries. *Sports Med* **42,** 209-226.

Owens DJ, Sharples AP, Polydorou I, Alwan N, Donovan T, Tang J, Fraser WD, Cooper RG, Morton JP & Stewart C. (2015). A systems-based investigation into vitamin D and skeletal muscle repair, regeneration, and hypertrophy. *Am J Physiol-Endoc M* **309,** E1019-E1031.

Paschalis V, Giakas G, Baltzopoulos V, Jamurtas AZ, Theoharis V, Kotzamanidis C & Koutedakis Y. (2007). The effects of muscle damage following eccentric exercise on gait biomechanics. *Gait & posture* **25,** 236-242.

Reeves ND, Narici MV & Maganaris CN. (2004). In vivo human muscle structure and function: adaptations to resistance training in old age. *Experimental physiology* **89,** 675-689.

Robinson MA & Vanrenterghem J. (2012). An evaluation of anatomical and functional knee axis definition in the context of side-cutting. *Journal of biomechanics* **45,** 1941-1946.

Schuermans J, Van Tiggelen D, Danneels L & Witvrouw E. (2014). Biceps femoris and semitendinosus—teammates or competitors? New insights into hamstring injury mechanisms in male football players: a muscle functional MRI study. *Br J Sports Med* **48,** 1599-1606.

Schwartz MH & Rozumalski A. (2005). A new method for estimating joint parameters from motion data. *Journal of biomechanics* **38,** 107-116.

Scott J & Huskisson E. (1979). Vertical or horizontal visual analogue scales. *Ann Rheum Dis* **38,** 560.

Seymore KD, Domire ZJ, DeVita P, Rider PM & Kulas AS. (2017). The effect of Nordic hamstring strength training on muscle architecture, stiffness, and strength. *Eur J Appl Physiol* **117,** 943-953.

Stauber W, Clarkson P, Fritz V & Evans W. (1990). Extracellular matrix disruption and pain after eccentric muscle action. *J Appl Physiol* **69,** 868-874.

Stewart JD, Masi TL, Cumming AE, Molnar GM, Wentworth BM, Sampath K, McPherson JM & Yaeger PC. (2003). Characterization of proliferating human skeletal muscle-derived cells in vitro: Differential modulation of myoblast markers by TGF-β2. *J Cell Physio* **196,** 70-78.

Terry EE, Zhang X, Hoffmann C, Hughes LD, Lewis SA, Li J, Wallace MJ, Riley LA, Douglas CM & Gutierrez-Monreal MA. (2018). Transcriptional profiling reveals extraordinary diversity among skeletal muscle tissues. *eLife* **7**.

Thelen DG, Chumanov ES, Hoerth DM, Best TM, Swanson SC, Li L, Young M & Heiderscheit BC. (2005). Hamstring muscle kinematics during treadmill sprinting. *Medicine and science in sports and exercise* **37,** 108-114.

Tidball JG. (2011). Mechanisms of muscle injury, repair, and regeneration. *Comprehensive Physiology* **1,** 2029-2062.

Timmins RG, Bourne MN, Shield AJ, Williams MD, Lorenzen C & Opar DA. (2015). Short biceps femoris fascicles and eccentric knee flexor weakness increase the risk of hamstring injury in elite football (soccer): a prospective cohort study. *Br J Sports Med***,** bjsports-2015-095362.

Timmins RG, Bourne MN, Shield AJ, Williams MD, Lorenzen C & Opar DA. (2016a). Short biceps femoris fascicles and eccentric knee flexor weakness increase the risk of hamstring injury in elite football (soccer): a prospective cohort study. *Br J Sports Med* **50,** 1524-1535.

Timmins RG, Opar DA, WIlliams MD, Schache AG, Dear NM & Shield AJ. (2014). Reduced biceps femoris myoelectrical activity influences eccentric knee flexor weakness after repeat sprint running. *Scandinavian journal of medicine & science in sports* **24,** e299-e305.

Timmins RG, Shield AJ, Williams MD, Lorenzen C & Opar DA. (2016b). Architectural adaptations of muscle to training and injury: a narrative review outlining the contributions by fascicle length, pennation angle and muscle thickness. *Br J Sports Med***,** bjsports-2015-094881.

Turrina A, Martínez-González MA & Stecco C. (2013). The muscular force transmission system: role of the intramuscular connective tissue. *J Bodywork Movement Ther* **17,** 95-102.

Valle X, Alentorn-Geli E, Tol JL, Hamilton B, Garrett WE, Pruna R, Til L, Gutierrez JA, Alomar X & Balius R. (2017). Muscle injuries in sports: a new evidence-informed and expert consensus-based classification with clinical application. *Sports Med* **47,** 1241-1253.

van der Horst N, Smits D-W, Petersen J, Goedhart EA & Backx FJ. (2015). The Preventive Effect of the Nordic Hamstring Exercise on Hamstring Injuries in Amateur Soccer Players A Randomized Controlled Trial. *The American journal of sports medicine***,** 0363546515574057.

van Dyk N, Bahr R, Whiteley R, Tol JL, Kumar BD, Hamilton B, Farooq A & Witvrouw E. (2016). Hamstring and Quadriceps Isokinetic Strength Deficits Are Weak Risk Factors for Hamstring Strain Injuries A 4-Year Cohort Study. *The American journal of sports medicine***,** 0363546516632526.

Verheul J, Clansey AC & Lake MJ. (2017). Adjustments with running speed reveal neuromuscular adaptations during landing associated with high mileage running training. *Journal of applied physiology* **122,** 653-665.

Verma S, Moiz J, Shareef M & Husain M. (2015). Physical performance and markers of muscle damage following sports specific sprints in male collegiate soccer players: repeated bout effect. *The Journal of sports medicine and physical fitness*.

Wang N, Tytell JD & Ingber DE. (2009). Mechanotransduction at a distance: mechanically coupling the extracellular matrix with the nucleus. *Nature reviews Molecular cell biology* **10,** 75-82.

Woods K, Bishop P & Jones E. (2007). Warm-up and stretching in the prevention of muscular injury. *Sports Med* **37,** 1089-1099.

Wüst RC, Morse CI, De Haan A, Jones DA & Degens H. (2008). Sex differences in contractile properties and fatigue resistance of human skeletal muscle. *Experimental physiology* **93,** 843-850.

SUPPLEMENTARY INFORMATION

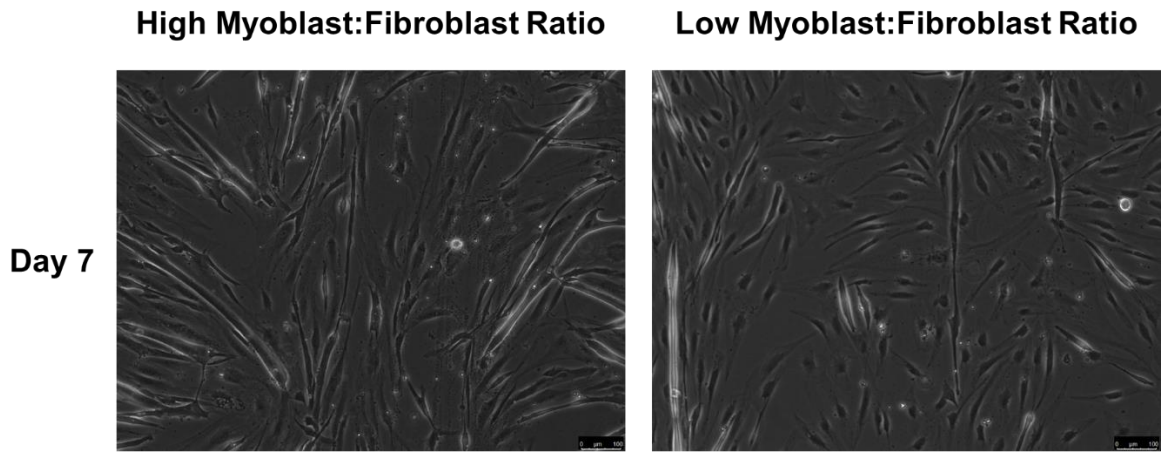

Figure supplement 5 *Representative images for muscle cell differentiation with a high myoblast:fibroblast ratio (2.4; left) and with a low myoblast:fibroblast ratio (0.3; right) at day seven. Magnification is x 10.5, and scale bar is 100 µm.*

Table supplement 4 Architectural parameters of biceps femoris long head (mean ± SD).

Muscle length [cm]	Fascicle length [cm]	PCSA [cm^2]	Volume [cm^3]	Fascicle Pennation Angle [°]
27.86 ± 2.13	7.94 ± 1.38	23.4 ± 4.62	182.2 ± 29.5	12.7 ± 2.77

Fascicle length at 50% of BF_{LH} muscle length; PCSA – Physiological cross-sectional area.

1107 ***Table supplement 6*** *Linear regression analysis between the myoblast:fibroblast ratio and fusion*
1108 *parameters at day 7 and CK activity at day 10 in vitro*.

	R^2	F-Test	P Value
Total myotubes [n]	0.345	F(1,10) = 5.27	0.045*
Myotube Length [µm]	0.339	F(1,10) = 5.13	0.047*
Myotube Diameter [µm]	0.387	F(1,10) = 5.56	0.031*
Myotube Area [μm^2]	0.404	F(1,10) = 6.79	0.026*
CK activity [mU/mL]	0.409	F(1,10) = 6.23	0.034*

* significant (P<0.05);

1109